Comprehensive Modelling of the Self-Folding Cavitand Dynamics

Ricard López-Coll, Rubén Álvarez-Yebra, Ferran Feixas,* Agustí Lledó*

Institut de Química Computacional i Catàlisi (IQCC), Universitat de Girona, c/M. Aurèlia Capmany 69, 17003, Girona, Spain.

ABSTRACT: The conformational equilibria and guest exchange process of a resorcin[4]arene derived self-folding cavitand receptor have been modelled in detail by molecular dynamics simulations (MD). A multi-timescale strategy for exploring the fluxional behavior of this system has been constructed, exploiting conventional MD and accelerated MD (aMD) techniques. The use of aMD allows the reconstruction of the folding/unfolding process of the receptor by sampling high-energy barrier processes unattainable by conventional MD simulations. We obtained MD trajectories sampling events occurring at different timescales: 1) rearrangement of the directional hydrogen bond seam stabilizing the receptor, 2) folding/unfolding of the structure transiting partially open intermediates, and c) guest departure from different folding stages. Most remarkably, reweighing of the biased aMD simulations provided kinetic barriers that are in very good agreement with those determined experimentally by ^{1}H NMR. These results constitute the first comprehensive computational characterization of the complex dynamic features of cavitand receptors. Our approach emerges as a valuable rational design tool for synthetic host-guest systems.

INTRODUCTION

The term cavitand was coined by Cram and co-workers in 1982 to describe "synthetic organic compounds that contain enforced cavities large enough to accommodate simple molecules or ions".[1] Ever since, this definition has been preferentially used for receptors obtained by covalently bridging the phenolic moieties of resorcin[4]arenes with aromatic spacers. In 1997, Rebek and co-workers introduced a significant improvement of this concept and synthesized the first self-folding cavitands, in which the binding-competent closed conformation of the receptor is stabilized by a seam of cooperative hydrogen bonding interactions between amide groups on the open rim of the cavitand (**1**, Figure 1).[2] As a result, host-guest equilibria are slowed down significantly, allowing the guests to remain longer in the confined space of the receptor. This feature has been exploited to isolate elusive reactive intermediates and develop biomimetic catalysis with properly functionalized cavitands (**IA**, Figure 1).[3] Inspiration from nature has been historically the main drive in the development of supramolecular catalysis,[4] and we have focused in the last years in developing new functionalized receptors for this purpose.[5] With notable exceptions, the *de novo* development of supramolecular catalysis with cavitands and analogous receptors is plagued with a number of impediments, such as product inhibition.[6] The design of appropriate guests or substrates is also far from trivial, and relies primarily on qualitative and empirical considerations such as the 55% rule, of uncertain validity for open-end containers.[7] In this scenario, the use of computational tools

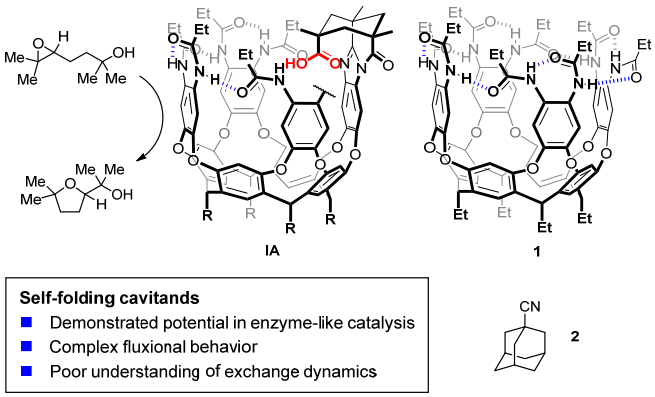

Figure 1. The self-folding introverted acid cavitand (**IA**) displays enzyme like catalysis of epoxy-alcohol cyclization reactions. The self-folding parent cavitand structure **1** is used in this work to study the guest exchange dynamics of these systems, in combination with 1-adamantanecarbonitrile (**2**) as a guest.

appears as a necessity to unveil the bases of the molecular recognition events that govern these systems. Only then can these first principles be applied in the rational design of new host-guest systems suitable for catalytic applications.

A number of theoretical studies on resorcinarene-derived receptors have been reported, mostly based on the characterization of stationary points employing ab-initio methods.[8] Arguably, this approach fails to grasp the complex dynamic nature that is intrinsic to most host-guest systems.

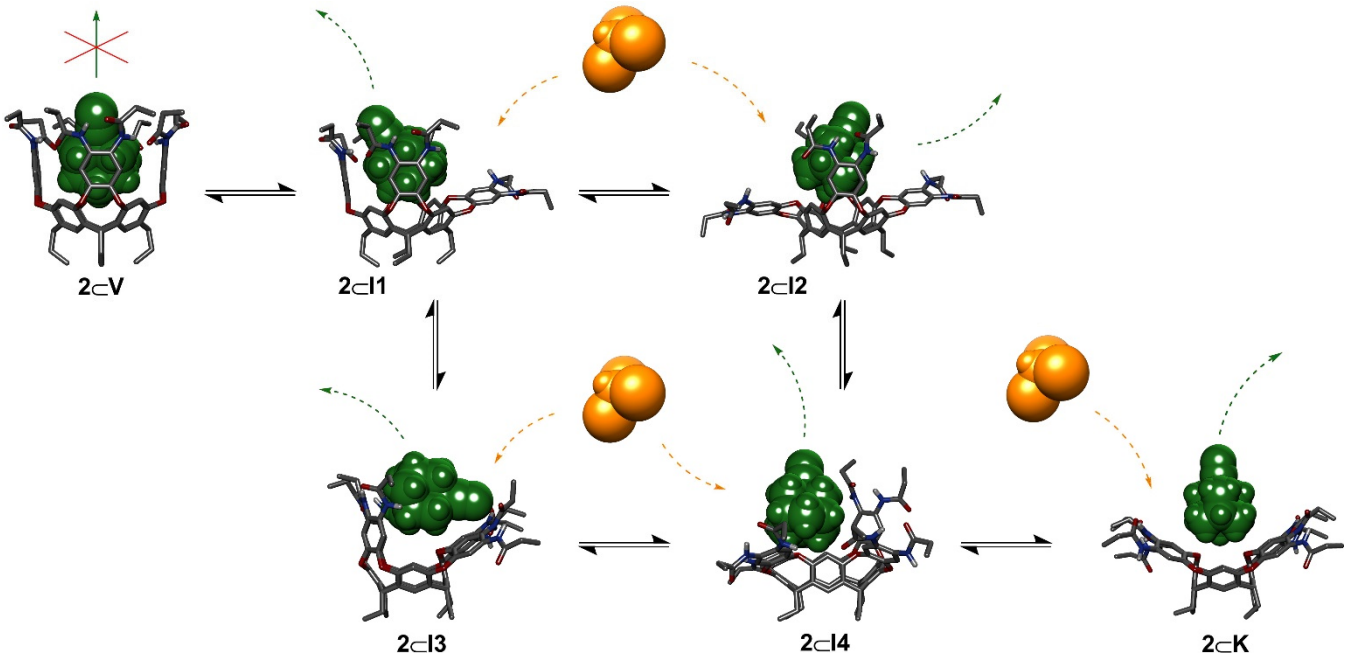

Scheme 1. All possible conformational equilibria involved in cavitand folding/unfolding and guest exchange. The arrows depict potential guest exchange by solvent molecules. Green: 1-adamantanecarbonitrile; orange: chloroform. The structures have been optimized at the semiempirical PM6 level of theory, including solvent effect corrections of chloroform solution.

Cavitands, for instance, are capable of displaying a range of different conformations in solution, and this fluxional behaviour is key for the molecular recognition process. However, this intrinsic flexibility remains unexplored on the molecular detail. Given the established parallels of self-folding cavitands with enzymatic receptors, we propose to use Molecular Dynamics (MD) simulations –the method of choice for modelling protein dynamics– to reconstruct in detail the binding and exchange dynamics of the said host-guest complexes, laying the foundations for a universal and computationally guided approach to the design of synthetic host guest systems for different purposes, including supramolecular catalysis.[9]

Self-folding cavitand receptors display conformational and guest exchange processes with relatively high barriers (ΔG), in the range of 16-19 kcal mol^{-1},[10] corresponding to timescales of milliseconds to seconds.[11] These timescales are still not accessible for conventional MD simulations: low-energy states relevant to these processes are separated by high-energy barriers in the free-energy landscape, which are rarely crossed over the course of a single unbiased MD simulation. A proper depiction of a complex system involving motions with disparate energy barriers and time scales necessitates a combination of MD-based techniques tailored to these individual events, including enhanced sampling techniques for exploring transitions involving high barrier processes. In this regard MD simulations can be seen as a "computational microscope" with different "objectives" for each of the required time scales. Enhanced sampling techniques represent an attractive strategy to sample slow processes that cannot be explored by conventional MD simulations.[12] The basis of speeding up conformational sampling is the introduction of an artificial bias into the model upon which the MD simulations are based. Enhanced sampling methods can be divided into two groups: those based on biasing a set of collective variables (CVs), and unconstrained methods. Using a refined set of CVs, Pavan and co-workers recovered from metadynamics simulations the thermodynamic and kinetics of guest binding and release in a coordination cage obtaining results in agreement with experimental values.[13] However, the identification of appropriate CVs can become complex when relevant states in the studied process remain hidden. Among the unconstrained methods, accelerated molecular dynamics (aMD) is particularly appealing because it does not rely on the *a priori* definition of a set of CVs and, therefore, provides unconstrained enhanced sampling to freely explore the molecular conformational space.[14] aMD enhances conformational sampling by adding a non-negative boost potential to the system when the system potential is lower than a reference energy. Recently, aMD simulations have been successfully employed to explore the folding pathways of small proteins, and to reconstruct substrate binding in enzymatic and supramolecular receptors.[15] Herein, we apply for the first time accelerated molecular dynamics (aMD), in combination with conventional MD, to describe in full the conformational and guest exchange dynamics of the prototypical self-folding cavitand **1**, using 1-adamantanecarbonitrile (**2**) as guest in chloroform solution.

RESULTS AND DISCUSSION

Self-folding cavitands such as **1** display a distinct conformational behaviour (Scheme 1). Two extreme conformations exist: the vase form or closed conformer, which is competent for binding smaller complementary

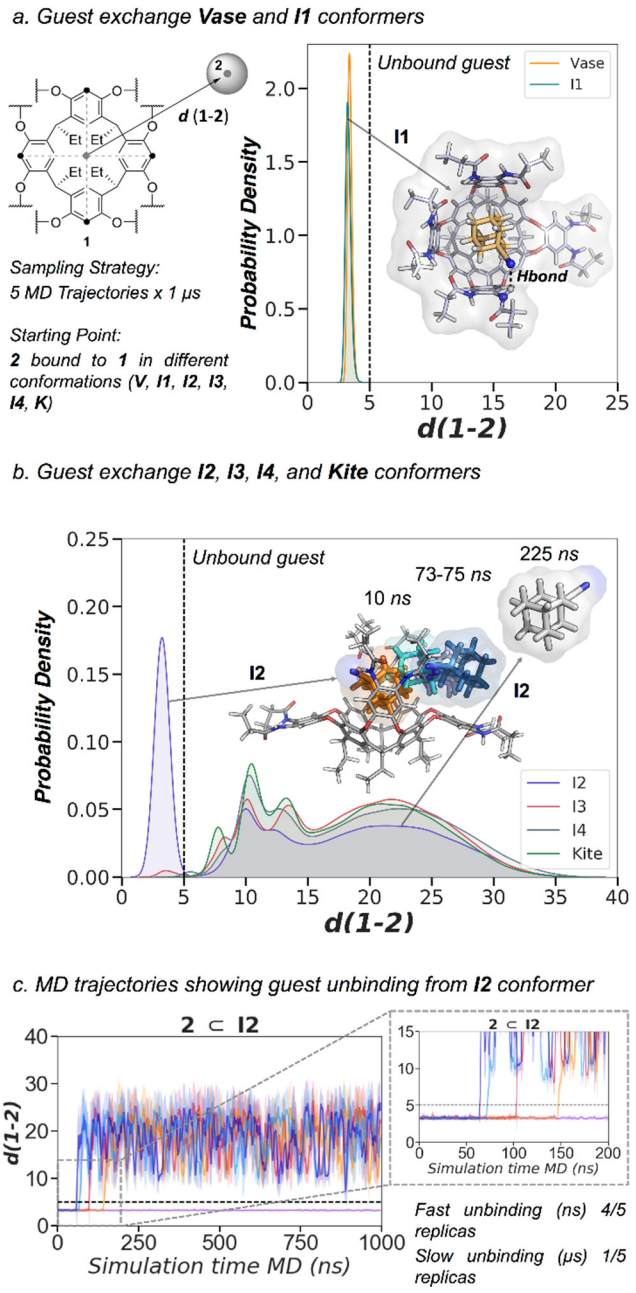

Figure 2. a) Schematic illustration of the distance d(**1**-**2**) used to monitor guest departure. Probability density distribution of d(**1**-**2**) for the vase (orange) and **I1** (teal) conformers. Distances above 5 Å indicate guest **2** unbinding. Representative snapshot of **I1** MD trajectory with the hydrogen bond between the cyano group of **2** and NH amide of **1** highlighted in black. b) Probability density distribution of d(**1**-**2**) for the **I2** (purple), **I3** (red), **I4** (gray), and kite (green) conformers. Representative snapshots of an MD trajectory of guest exchange for **I2** conformer. Frames are displayed at 10 (orange), 73 (cyan), 74 (light purple), 75 (dark blue), and 225 ns (white). c) Plot of the distance d(**1**-**2**) (Å) along the MD trajectories of **I2** conformer. The distance is monitored for five 1 μs replicas (shown in different colours). A 5 Å threshold is shown to highlight guest departure.

molecules, and the kite open conformer.[16] The latter features an extended flat aromatic surface and is ripe for self-aggregation through π-stacking interactions. The resulting *velcrand* dimer prevails over higher order aggregates, and is devoid of further molecular recognition properties. Guest exchange is in slow regime compared to the NMR time scale, producing two sets of signals for bound and unbound guest resonances. The bound guest's resonances experience large anisotropic shielding from the cumulative effect of 8 aromatic panels, resulting in large upfield shifts. As a result, aliphatic protons on the guest appear in the far upfield region of the ^{1}H NMR spectrum, which is devoid of interference by the host's resonances. This feature facilitates analysis of the exchange kinetics, and allows extraction of exchange rates and barriers through EXSY experiments.[10] Importantly, no stable intermediates of the exchange process are observed in solution by ^{1}H NMR. However, host-guest intermediate structures in which one, two, or three walls of the cavitand have flipped out can be located as stable local minima by means of semiempirical calculations (Scheme 1).

Guest exchange

The following model has been proposed for guest exchange. Direct removal of the guest from the vase form (**V**, Scheme 1) is not viable: it would generate a void behind. Direct substitution by another guest molecule without unfolding –as in an S_N2 substitution– is also unlikely, because of the crowded environment around the bound guest. An alternative scenario involves unfolding of the cavitand's walls and exposure of the guest to the surrounding medium, triggering the exchange by another guest or solvent molecule. To its extreme, this process would be akin to an S_N1 substitution in terms of the potential energy surface, the initial unfolding being a slow, rate-determining step followed by a rapid, barrier-less guest replacement. The question remains, however, how many walls must flip before the guest can freely diffuse out? To ascertain this we performed conventional MD simulations of the molecular complex of **2** with **1** in its different states, including partially open intermediates (Scheme 1): vase (**V**), one wall open (**I1**), two opposing walls open (**I2**), two adjacent walls open (**I3**), three walls open (**I4**) and kite (**K**). We employed as starting geometries the PM6-optimized molecular complexes of **2** with the different conformers of **1** (Scheme 1). In total, five replicas of 1 μs of MD simulations for each system were carried out, gathering a total simulation time of 30 μs. The resulting trajectories reveal that the conformational transitions involved in the unfolding process (*wall flips*) are not accessible in this microsecond time scale (see SI), and confirms that the guest cannot escape from the vase conformer (Figure 2). In the closed conformer, the guest freely rotates inside the cavitand with the cyano group of the guest establishing transient hydrogen bonds with the amide groups. To illustrate and compare the guest exchange step along the simulations of different conformers, we monitored the distance between the centre of mass of guest **2** and the centre of the 4 upper carbons on the resorcinarene core of cavitand **1**, d(**1**-**2**) (Figure 2). As with the vase conformer (**V**), the guest also remains in the

cavity for the duration of the simulation with conformer **I1**, which is in good agreement with the fact that cavitands lacking a 4th wall provide kinetically stable host-guest complexes in the microsecond time-scale.[10a, 17] In this particular case, the guest is retained inside the host by means of hydrophobic interactions with the aromatic panels, and by a relatively stable hydrogen bond between the cyano group and an amide NH that remains available because of the removed wall. Interestingly, conformers with only two walls open (**I2**, **I3**) allow guest replacement by solvent molecules in these simulations, with a clear transition of **2** from bound to unbound occurring in the range of 60-140 and 5-20 ns respectively (Figures 2c and S3). The conformer with two opposing walls open (**I2**) has better shape complementarity for **2**, and establishes stronger interactions with the guest than **I3**. In one of the replicas calculated for **I2**, the guest remains bound between the closed aromatic panels for the duration of entire simulation (1 μs). For comparison, the trajectories for conformers **I4** and **K** (kite) display guest **2** freely diffusing away from **1** from the very first frames of the simulation (during the equilibration phase actually), indicating a barrier-less scenario. Our results point out that the conformational equilibrium between **I1** and **I2** can play a key role on guest exchange and molecular recognition.

Amide flip: cycloenantiomer interconversion

Having established that cavitand unfolding requires access to high energy states not populated in the course of conventional MD simulations, we resorted to enhanced sampling techniques in order to explore the wall flip transitions that regulate folding and, ultimately, the overall guest exchange process. We applied aMD to simulate host **1** in the vase conformer using chloroform as a solvent and guest. At the onset, an average dihedral boost potential of 115 kcal mol^{-1} was applied through 14 μs of aMD simulation time. This simulation protocol allows for an extensive conformational sampling of the folded state of the cavitand. During the course of this simulation no wall flip transitions were observed. Two chloroform molecules are accommodated at the wider open end of the container, which are continuously replaced by molecules of the solvent cage throughout the simulation. A third molecule of chloroform that is bound at the tapered end of **V** in the beginning of the simulation remains inside the cavity during the whole aMD trajectory. Therefore, we can consider that guest exchange is not observed under these conditions. However, an interesting concerted motion of the amide groups forming the hydrogen bond seam is captured (Figure 3). The hydrogen bond seam defined by the amide groups is directional, imparting C_4 symmetry to the cavitand structure. Rotation about the aryl-nitrogen bond of all the amide groups provides two cycloenantiomeric forms, (*Δ*)-**V** and (*Λ*)-**V**, of the cavitand (Figure 3). The carbonyl groups are arranged clockwise (C to O) in the *Δ* enantiomer and anti-clockwise in the *Λ* enantiomer. These cycloenantiomers can interconvert by unfolding followed by amide rotation about the aryl-N

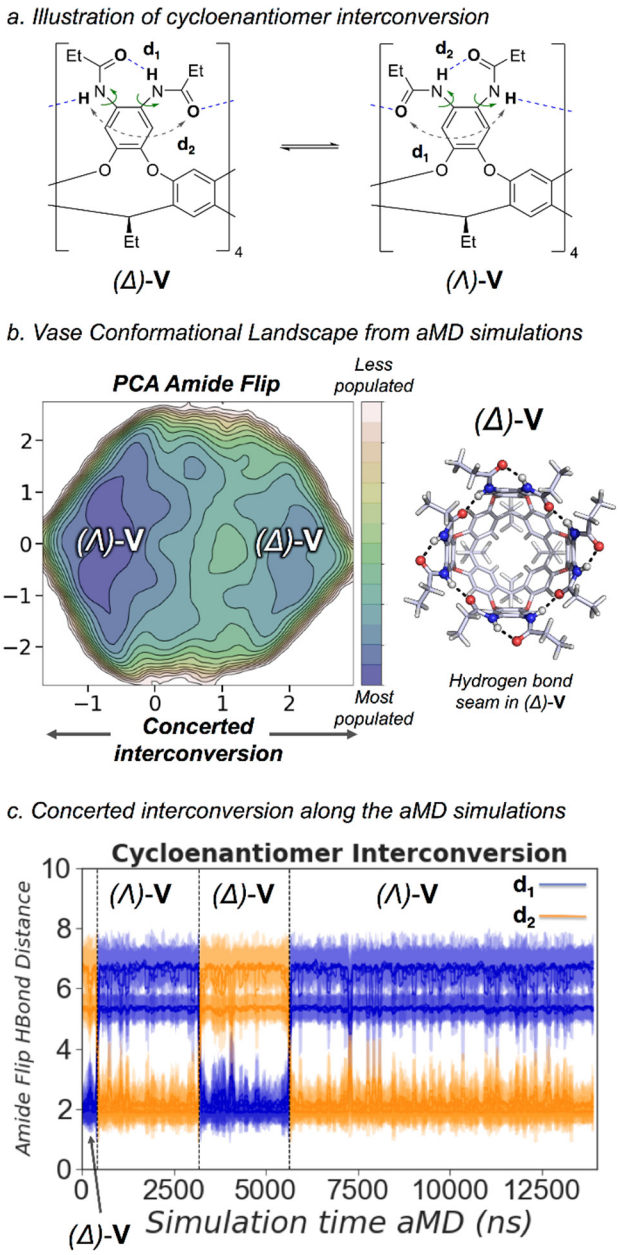

Figure 3. a) Schematic illustration of cycloenantiomer interconversion highlighting the relevant aryl-N bond rotation and NH···O distances. b) Reconstructed Conformational Landscape obtained from the PCA of accumulated simulation time of 14 μs of aMD simulations. PC1 describes the concerted motion of the eight hydrogen bonds forming the seam of the vase conformer. c) Distance plot of the two possible hydrogen bonding arrangements of each aromatic panel represented by NH···O distances d_1 and d_2 (Å), along the aMD trajectory. The plot contains the eight hydrogen bond distances in **V**.

bond and refolding. However, the aMD simulations unveil a concerted motion of the 8 amide groups that interconverts the cycloenantiomers without any wall flipping out (Figure 3). To describe the nature of this interconversion in more detail, we reconstructed the conformational landscape by applying principal

component analysis (PCA, see computational details section) to our aMD simulation (Figure 3b). Interestingly, the reconstructed conformational landscape reveals only two symmetric minima. The inspection of the structures belonging to each free energy basin shows that one minimum corresponds to (*Δ*)-**V** and the other to its cycloenantiomer (*Λ*)-**V**. The absence of additional metastable minima showcases the fast concerted interconversion of the whole hydrogen bond network formed by the amide groups. The structures located in the transition region between (*Δ*)-**V** and (*Λ*)-**V** remain in vase-like conformations, indicating that the interconversion takes place without partial unfolding. A detailed analysis along the aMD trajectory of the NH···O distances involved in hydrogen bonding (d1 and d2, Figure 3a) shows that three transitions are observed in the timespan of the 14 μs aMD simulation (Figure 3c). Distances d1 and d2 alternate between ca. 2 and 5-7 Å upon amide rotation. The cycloreversion process must have a significantly lower energy barrier than any unfolding motion, not observed throughout the simulations under these conditions. It is known that aMD simulations of a few microseconds of are able to capture millisecond-timescale events in proteins.[12b] The reweighting of the aMD simulations reveals a cycloenantiomer interconversion barrier of nearly 14.5 kcal mol^{-1} (Figure S4). All these observations are in good agreement with the fact that host-guest complexes of **1** in hydrogen bonding solvents –such as acetone-d_6–, retain slow guest exchange kinetics (in the NMR time scale), while displaying fast exchange for the amide NH resonances.[10a] On the contrary, our findings collide with the seminal work of Rebek, who reported coincident barriers for both the amide flip motion and the guest exchange process, in this case in a non-competitive apolar solvent (mesitylene-d_{12}).[2b] Given the fact that those exchange barriers were extracted in part from coalescence experiments, we decided to re-evaluate them experimentally employing only the more accurate and well-established EXSY experiment.[10, 18] We assessed the 1st order rate constants for the amide flip of **1** in $CDCl_3$, and for the guest dissociation processes of **2⊂1** in the same solvent. For accuracy, we carried out ^{1}H EXSY experiments at different temperatures, and extracted the activation parameters by Eyring analysis of the rate constants at different temperatures (Figure 4). Extrapolation to 300 K gave exchange barriers ΔG of 13.5 and 20.0 kcal mol^{-1} for the amide flip and guest exchange respectively. These results point to significant rate differences between the two processes, even in a non-hydrogen-bonding solvent, in very good agreement with our aMD simulations. Remarkably, the calculated barrier for the amide flip motion is within 1 kcal mol^{-1} difference of the experimentally determined value.

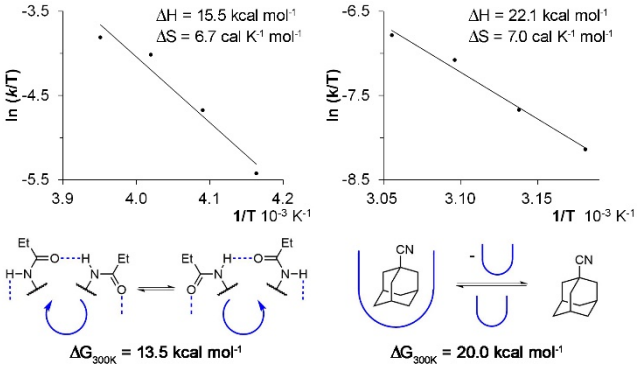

Figure 4. Eyring plots, activation parameters and free energy barriers at 300 K for the amide flip (left) and guest exchange processes.

Cavitand folding and unfolding

Wall flip motions leading to unfolding or folding of the cavitand structure involve synchronous rotation of multiple dihedral angles restricted by the bridging aromatic panels. The guest exchange barrier of 20 kcal mol^{-1} determined experimentally is indicative of the energetic cost of the folding and unfolding process. In order to populate the high energy states involved in folding and cross the high energy barriers required for wall flipping, we first performed aMD simulations using significantly larger dihedral boost potentials than those used for the study of the amide flip motion. We submitted a series of 1 μs aMD simulations starting from the six conformers (**V**, **I1**, **I2**, **I3**, **I4**, and **K**) in a chloroform solvent cage and a chloroform molecule as the guest, and found out that dihedral boost potentials in excess of 1000 kcal mol^{-1} were necessary to sample the correlated torsions required for folding. All aMD simulations converged to the vase conformer irrespective of the starting geometry, suggesting that the most populated state in solution is the vase. This observation is in good agreement with the established notion that the folded conformer is significantly more stable than the others in solution. While these forceful aMD simulations provided a qualitative picture of the self-folding process, the high and physically unrealistic average boost potentials applied prevented any kind of quantitative assessment of the folding process. A qualitative inspection of the resulting trajectories at the molecular level revealed abundant aberrant motions (e.g. exacerbated out of plane torsions in aromatic rings), corroborating that further analysis of metastable intermediates is not possible with this coarse model. To overcome this shortcoming, we set out to tailor the aMD technique to our problem. Unfortunately, previous applications to synthetic host-guest systems using specific set of acceleration parameters are virtually non-existent. The main difficulty is that aMD was originally developed for proteins, and the range of E (reference value) and α (acceleration factor) parameters that are relevant to acceleration is neither benchmarked nor fitted for non-proteinogenic systems.[14] Additionally, the connection of E and α to the outcoming boost and how the forces are rescaled (force weight, FW) is undetermined.

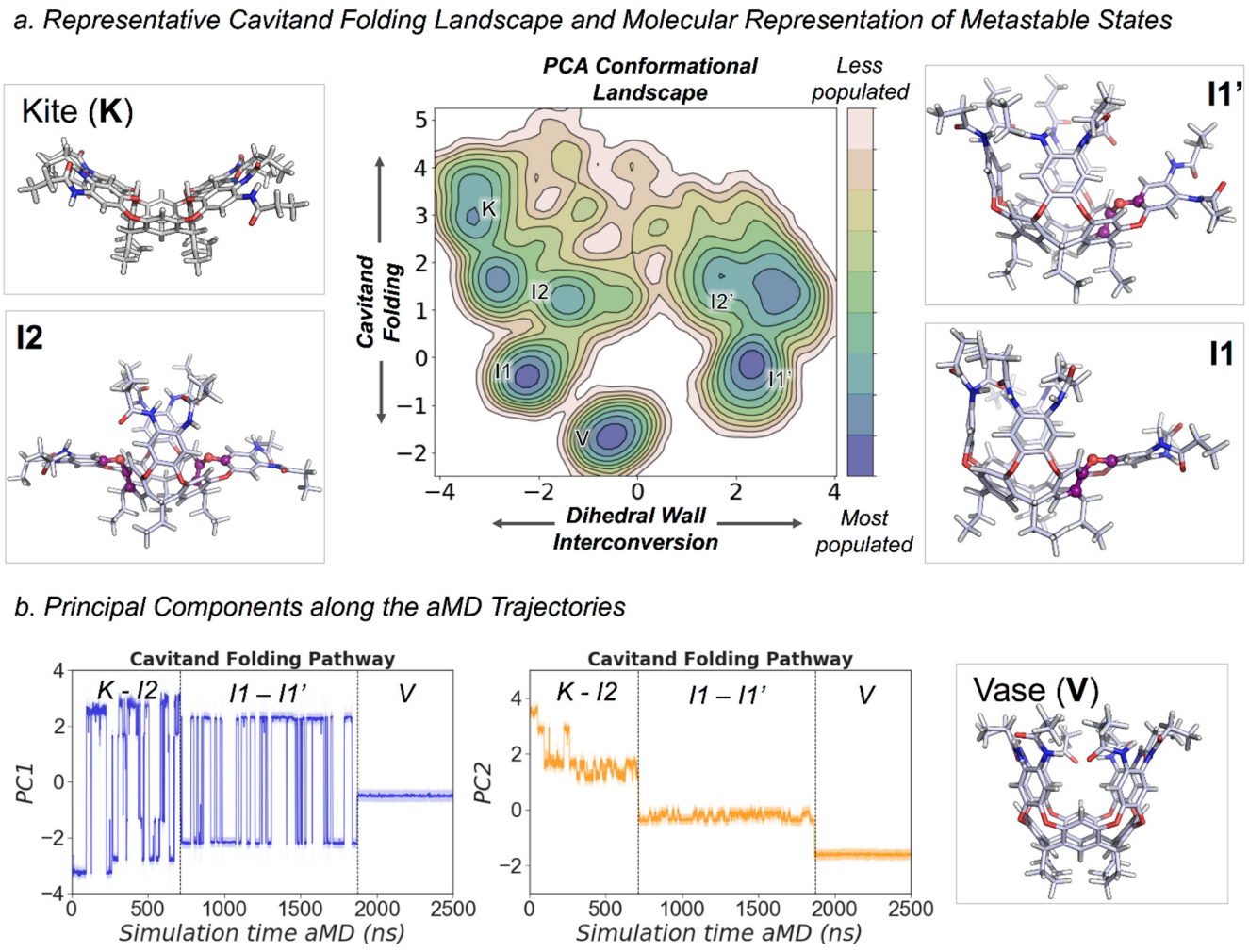

Figure 5. a) Illustration of cavitand folding pathways. Reconstructed conformational landscape obtained from principal component analysis of dihedral angles of bridging aromatic groups of an accumulated simulation time of 2.5 μs of aMD simulations starting from **K**. PC1 represents the concerted rotation of the two dihedrals comprising a single wall without involving the flip of the wall. PC2 is directly related to the self-folding event, connecting the **K**, **I2**, **I1** and **V** conformers characterized by the progressive wall flipping. The most representative structures are highlighted. b) Plot of two principal components along the aMD trajectory.

To address this, we screened a large number of different E/α combinations starting from different conformers of **1**. After much experimentation, we found a set of parameters that enabled the gentle sampling of the full conformational transition, from **K** to **V**, with a moderate average dihedral boost potential of 160 kcal mol^{-1} and total boost potential of 170 kcal mol^{-1}. Five 2.5 μs simulation replicas where run under this optimized conditions, providing reproducible results and identical outcome. Following the trend indicated by our preliminary aMD analysis, all simulations spontaneously converge to the vase conformer (**V**) with a chloroform molecule occupying the centre of the cavity. Under these refined conditions, smooth conformational changes leading to the closure of the cavitand are revealed, transiting through a series of interconnected metastable states.

In order to visualize and understand the folding pathway, we reconstructed the conformational landscape of the kite (**K**) to vase (**V**) folding process by applying PCA to our aMD simulations using the dihedral angles of the bridging aromatic panels as features (Figure 5, see computational details section). The first two principal components clearly differentiate between unfolded and folded states. PC2 is directly related to the self-folding event, connecting the **K**, **I2**, **I1** and **V** conformers characterized by the progressive wall flipping. PC1 represents the concerted rotation of the two dihedrals comprising a single wall without involving the flip of the wall. Moreover, we are able to identify in the resulting conformational landscape several key intermediate states that connect the kite and vase conformations. Some of them are similar the minima previously obtained by means of semiempirical calculations, but other relevant states are also populated including additional **I1**- and **I2**-like conformers (Figures 5 and S6). As a general trend, we observed that the folding pathway involves an initial transition from kite-like states to **I2**, where two opposite walls move up, trapping chloroform molecules in between. Then, the two remaining open walls fold in a step-wise fashion, populating first **I1** and finally **V**. Interestingly, the

PCA analysis reveals a conformational equilibrium along PC1 between **I1** and **I1'** conformers. These two metastable states differ on the dihedral angle that remains unflipped in a particular wall. The concerted interconversion between these two forms precedes the formation of **V**. Once the **V** form is attained, multiple amide flips are observed without unfolding of the cavitand structure. The reweighting of the aMD simulations along PC2 indicates that the barrier that separates **I2** and **V** is roughly 20 kcal mol^{-1} (see SI), 5.5 kcal mol^{-1} higher than the one obtained for the cycloenantiomer interconversion. These values are in very good agreement with the EXSY experiments, which indicate a similar difference between the guest exchange and the amide flip barriers (ΔΔG). Our results corroborate that unfolding of at least two panels (as in **I2**) is required to complete the guest exchange process.

CONCLUSIONS

We have reproduced the guest exchange and conformational equilibria of stabilized self-folding cavitand **1** with MD simulations. We applied for the first time aMD techniques and long MD trajectories to self-folding cavitands, allowing sampling of high-energy states and conformational barriers. The aMD simulations reveal a series of hidden states not located as stationary points. Overall, our multi-timescale simulations provide an accurate description of the folding, unfolding and guest exchange processes of amide stabilized self-folding cavitands in very good agreement with experimentally determined kinetic barriers. While aMD provides excellent conformational sampling, it usually suffers in estimating the free energy barriers between different states of a large system (open/closed or bound/unbound). Our work demonstrates for the first time the use of aMD for obtaining a quantitative model of a dynamically complex host-guest system. This method should find applicability in other systems of similar complexity, and thus become a valuable tool for the rational design of functional synthetic hosts.

EXPERIMENTAL SECTION

Cavitand **1** was prepared following established procedures.[19] 1-Adamantanecarbonitrile (**2**, 97%) was purchased from Sigma-Aldrich, and used as received. Details for the EXSY experiments and the calculation of the exchange rates are provided in the supporting information.

Computational details

Geometries of the starting stationary points for MD simulations (conformers **V**, **I1**-**I4**, **K**) with **2** as a guest were optimized without symmetry constraints with the Gaussian 09 program[20] at the semiempirical PM6 level, including solvent effects corrections of chloroform solution computed with the polarizable continuum solvation model (PCM).[21]

Host-Guest parameterization. The MD simulation parameters for **1** and **2** were generated within the ANTECHAMBER module of AMBER 16 using the upgraded version of the general AMBER force field (GAFF2),[22] with partial charges calculated according to AM1-BCC scheme[23] using ANTECHAMBER.

Molecular Dynamics Simulations. Each system was immersed in a pre-equilibrated cubic box of chloroform molecules with an internal offset distance of 12 Å, using the AMBER 16 LEaP module. All calculations were done using the GAFF2 force field. A two-stage geometry optimization approach was performed. First, a short minimization of the chloroform molecules positions, with positional restraints on solute by a harmonic potential with a force constant of 500 kcal mol^{-1} $Å^{-2}$ was done. The second stage was an unrestrained minimization of all the atoms in the simulation cell. Then, the systems were heated using six 50 ps steps, incrementing the temperature 50 K each step (0-300 K) under constant-volume, periodic-boundary conditions and the particle-mesh Ewald approach[24] to introduce long-range electrostatic effects. For these steps, a 10 Å cut-off was applied to Lennard-Jones and electrostatic interactions. Bonds involving hydrogen were constrained with the SHAKE algorithm. Harmonic restraints of 10 kcal mol^{-1} were applied to the solute, and the Langevin equilibration scheme was used to control and equalize the temperature. The time step was kept at 2 fs during the heating stages, allowing potential inhomogeneities to self-adjust. Each system was then equilibrated for 2 ns with a 2 fs timestep at a constant pressure of 1 atm (NPT ensemble). Then MD simulations and aMD simulations were performed under the NVT ensemble and periodic-boundary conditions. In total, five replicas of 1 μs each of MD starting from 6 different conformers (**V**, **I1**, **I2**, **I3**, **I4**, and **K**) have been performed with 1-adamantanecarbonitrile bound (gathering a total of 30 μs of MD simulation).

Accelerated Molecular Dynamics Simulations. Accelerated Molecular Dynamics simulations (aMD)[14] were used to explore the cavitand dynamics and folding process using **1** and chloroform molecules as guest. The starting geometries were generated from the final step of a previous 100 ns conventional MD simulation. aMD enhances the conformational sampling by adding a non-negative boost potential to the system when the system potential is lower than a reference energy. A dihedral boost potential of ca. 115 kcal mol^{-1} was applied to simulate the interconversion of cycloenantiomers, while a finely tuned dual-boost of ca. 325 kcal mol^{-1} was used to simulate the folding process (see SI for details). The exponential reweighting of the aMD simulations was performed using the PyReweighting toolkit.[25] One replica of 14 μs was used to characterize the cycloenantiomer interconversion. Five replicas of 1 μs each starting from 6 different conformers (**V**, **I1**, **I2**, **I3**, **I4**, and **K**) were performed to sample the folding pathway using high boost potential. Finally, five replicas of 2.5 μs of aMD each starting from **K** were carried out with finely tuned parameters to explore the complete folding pathway. The conformational landscape for the cycloenantiomer interconversion has been reconstructed from the accumulation of 14 μs of aMD simulations. The high dimensional aMD data was reduced using principal component analysis (PCA) considering all the atoms of the

cavitand. The conformational landscape for the folding and unfolding of the cavitand have been reconstructed from the accumulation 2.5 μs of aMD simulations starting from the kite conformer. The high dimensional aMD data was reduced using the principal component analysis (PCA) considering all the dihedral angles of the bridging aromatic panels (Figure S5).

ASSOCIATED CONTENT

Supporting Information. Structures of starting geometries[26] and of states populated during MD simulations, details for the MD and aMD simulations parametrization, details of the PCA analysis, representative MD trajectories in mpg format, details for the EXSY calculations.

AUTHOR INFORMATION

Corresponding Author

* F. Feixas ferran.feixas@udg.edu
* A. Lledó agusti.lledo@udg.edu

Author Contributions

The manuscript was written through contributions of all authors. All authors have given approval to the final version of the manuscript.

ACKNOWLEDGMENT

We are grateful for financial support from the Spanish government ("Ramón y Cajal" contract RYC2012-11112 and grant CTQ2017-83587-P to A. L.; grant RTI2018-101032-J-I00 to F.F), the European Community (MSCA-IF-2014-EF-661160-MetAccembly grant to F.F), and the Generalitat de Catalunya (projects 2017-SGR-39 and 2017-SGR-1707). We thank the Spanish Supercomputing Network (RES) for access to supercomputing resources (projects QCM-2018-3-0036, QCM-2019-1-0022, and QSB-2020-1-0008).

REFERENCES

(1) Moran, J. R.; Karbach, S.; Cram, D. J., Cavitands: synthetic molecular vessels. *J. Am. Chem. Soc.* **1982,** *104* (21), 5826-5828.

(2) (a) Rudkevich, D. M.; Hilmersson, G.; Rebek, J., Self-Folding Cavitands. *J. Am. Chem. Soc.* **1998,** *120* (47), 12216-12225. (b) Rudkevich, D. M.; Hilmersson, G.; Rebek, J., Intramolecular Hydrogen Bonding Controls the Exchange Rates of Guests in a Cavitand. *J. Am. Chem. Soc.* **1997,** *119* (41), 9911-9912.

(3) (a) Hooley, R. J.; Rebek Jr, J., Chemistry and Catalysis in Functional Cavitands. *Chem. Biol.* **2009,** *16* (3), 255-264. (b) Pinacho Crisóstomo, F. R.; Lledó, A.; Shenoy, S. R.; Iwasawa, T.; Rebek, J., Recognition and Organocatalysis with a Synthetic Cavitand Receptor. *J. Am. Chem. Soc.* **2009,** *131* (21), 7402-7410.

(4) Raynal, M.; Ballester, P.; Vidal-Ferran, A.; van Leeuwen, P. W. N. M., Supramolecular catalysis. Part 2: artificial enzyme mimics. *Chem. Soc. Rev.* **2014,** *43* (5), 1734-1787.

(5) (a) Lledo, A.; Soler, A., Binding of ion pairs in a thiourea-functionalized self-folding cavitand. *Org. Chem. Front.* **2017,** *4* (7), 1244-1249. (b) Lledó, A., Complementary Binding in Urea-Based Self-Folding Cavitands. *Org. Lett.* **2015,** *17* (15), 3770-3773. (c) Vidal, D.; Costas, M.; Lledó, A., A Deep Cavitand Receptor Functionalized with Fe(II) and Mn(II) Aminopyridine Complexes for Bioinspired Oxidation Catalysis. *ACS Catal.* **2018,** *8* (4), 3667-3672.

(6) (a) Mosca, S.; Yu, Y.; Gavette, J. V.; Zhang, K.-D.; Rebek, J., A Deep Cavitand Templates Lactam Formation in Water. *J. Am. Chem. Soc.* **2015,** *137* (46), 14582-14585. (b) Butterfield, S. M.; Rebek Jr, J., A cavitand stabilizes the Meisenheimer complex of SNAr reactions. *Chem. Commun.* **2007,** (16), 1605-1607. (c) Purse, B. W.; Ballester, P.; Rebek, J., Reactivity and Molecular Recognition: Amine Methylation by an Introverted Ester. *J. Am. Chem. Soc.* **2003,** *125* (48), 14682-14683. (d) Chen, J.; Rebek, J., Selectivity in an Encapsulated Cycloaddition Reaction. *Org. Lett.* **2002,** *4* (3), 327-329.

(7) Mecozzi, S.; Rebek, J. J., The 55 % Solution: A Formula for Molecular Recognition in the Liquid State. *Chem. Eur. J.* **1998,** *4* (6), 1016-1022.

(8) (a) Xu, L.; Fang, G.; Tao, J.; Ye, Z.; Xu, S.; Li, Z., Molecular Mechanism and Solvation Effect of Supramolecular Catalysis in a Synthetic Cavitand Receptor with an Inwardly Directed Carboxylic Acid for Ring-Opening Cyclization of Epoxy Alcohols. *ACS Catal.* **2018**, 11910-11925. (b) Wu, N.-W.; Petsalakis, I. D.; Theodorakopoulos, G.; Yu, Y.; Rebek, J., Cavitands as Containers for α,ω-Dienes and Chaperones for Olefin Metathesis. *Angew. Chem. Int. Ed.* **2018,** *57* (46), 15091-15095. (c) Goehry, C.; Besora, M.; Maseras, F., Computational Description of a Huisgen Cycloaddition Inside a Self-Assembled Nanocapsule. *Eur. J. Org. Chem.* **2018,** *2018* (18), 2103-2109. (d) Daver, H.; Algarra, A. G.; Rebek, J.; Harvey, J. N.; Himo, F., Mixed Explicit–Implicit Solvation Approach for Modeling of Alkane Complexation in Water-Soluble Self-Assembled Capsules. *J. Am. Chem. Soc.* **2018,** *140* (39), 12527-12537. (e) Daver, H.; Harvey, J. N.; Rebek, J.; Himo, F., Quantum Chemical Modeling of Cycloaddition Reaction in a Self-Assembled Capsule. *J. Am. Chem. Soc.* **2017,** *139* (43), 15494-15503.

(9) Gottschalk, T.; Jaun, B.; Diederich, F., Container Molecules with Portals: Reversibly Switchable Cycloalkane Complexation. *Angew. Chem. Int. Ed.* **2007,** *46* (1-2), 260-264.

(10) (a) Lledo, A.; Rebek Jr, J., Self-folding cavitands: structural characterization of the induced-fit model. *Chem. Commun.* **2010,** *46* (10), 1637-1639. (b) Hooley, R. J.; Shenoy, S. R.; Rebek, J., Electronic and Steric Effects in Binding of Deep Cavitands. *Org. Lett.* **2008,** *10* (23), 5397-5400.

(11) Henzler-Wildman, K.; Kern, D., Dynamic personalities of proteins. *Nature* **2007,** *450*, 964.

(12) (a) Yang, Y. I.; Shao, Q.; Zhang, J.; Yang, L.; Gao, Y. Q., Enhanced sampling in molecular dynamics. *J. Chem. Phys.* **2019,** *151* (7), 070902. (b) McCammon, J. A., Unconstrained enhanced sampling for free energy calculations of biomolecules: a review AU - Miao, Yinglong. *Mol. Simul.* **2016,** *42* (13), 1046-1055.

(13) Pesce, L.; Perego, C.; Grommet, A. B.; Klajn, R.; Pavan, G. M., Molecular Factors Controlling the Isomerization of Azobenzenes in the Cavity of a Flexible Coordination Cage. *J. Am. Chem. Soc.* **2020,** *142* (21), 9792-9802.

(14) Hamelberg, D.; Mongan, J.; McCammon, J. A., Accelerated molecular dynamics: A promising and efficient simulation method for biomolecules. *J. Chem. Phys.* **2004,** *120* (24), 11919-11929.

(15) (a) Miao, Y.; Feixas, F.; Eun, C.; McCammon, J. A., Accelerated molecular dynamics simulations of protein folding. *J. Comput. Chem.* **2015,** *36* (20), 1536-1549. (b) Curado-Carballada, C.; Feixas, F.; Iglesias-Fernandez, J.; Osuna, S., Hidden Conformations in Aspergillus niger Monoamine Oxidase are Key for Catalytic Efficiency. *Angew. Chem. Int. Ed.* **2019,** *58* (10), 3097-3101. (c) García-Simón, C.; Colomban, C.; Çetin, Y. A.; Gimeno, A.; Pujals, M.; Ubasart, E.; Fuertes-Espinosa, C.; Asad, K.; Chronakis, N.; Costas, M.; Jiménez-Barbero, J.; Feixas, F.; Ribas, X., Complete Dynamic Reconstruction of C60, C70, and (C59N)2 Encapsulation into an Adaptable Supramolecular Nanocapsule. *J. Am. Chem. Soc.* **2020,** *142* (37), 16051-16063.

(16) Moran, J. R.; Ericson, J. L.; Dalcanale, E.; Bryant, J. A.; Knobler, C. B.; Cram, D. J., Vases and kites as cavitands. *J. Am. Chem. Soc.* **1991,** *113* (15), 5707-5714.

(17) (a) Lledó, A.; Hooley, R. J.; Rebek, J., Recognition of Guests by Water-Stabilized Cavitand Hosts. *Org. Lett.* **2008,** *10* (17), 3669-3671. (b) Ballester, P.; Sarmentero, M. A., Hybrid Cavitand–Resorcin[4]arene Receptor for the Selective Binding of Choline and Related Compounds in Protic Media. *Org. Lett.* **2006,** *8* (16), 3477-3480.

(18) Nikitin, K.; O'Gara, R., Mechanisms and Beyond: Elucidation of Fluxional Dynamics by Exchange NMR Spectroscopy. *Chem. Eur. J.* **2019,** *25* (18), 4551-4589.

(19) Purse, B. W.; Gissot, A.; Rebek, J., A Deep Cavitand Provides a Structured Environment for the Menschutkin Reaction. *J. Am. Chem. Soc.* **2005,** *127* (32), 11222-11223.

(20) Frisch, M. J.; Trucks, G. W.; Schlegel, H. B.; Scuseria, G. E.; Robb, M. A.; Cheeseman, J. R.; Scalmani, G.; Barone, V.; Mennucci, B.; Petersson, G. A.; Nakatsuji, H.; Caricato, M.; Li, X.; Hratchian, H. P.; Izmaylov, A. F.; Bloino, J.; Zheng, G.; Sonnenberg, J. L.; Hada, M.; Ehara, M.; Toyota, K.; Fukuda, R.; Hasegawa, J.; Ishida, M.; Nakajima, T.; Honda, Y.; Kitao, O.; Nakai, H.; Vreven, T.; Montgomery, J. A.; Peralta, J. E.; Ogliaro, F.; Bearpark, M.; Heyd, J. J.; Brothers, E.; Kudin, K. N.; Staroverov, V. N.; Kobayashi, R.; Normand, J.; Raghavachari, K.; Rendell, A.; Burant, J. C.; Iyengar, S. S.; Tomasi, J.; Cossi, M.; Rega, N.; Millam, J. M.; Klene, M.; Knox, J. E.; Cross, J. B.; Bakken, V.; Adamo, C.; Jaramillo, J.; Gomperts, R.; Stratmann, R. E.; Yazyev, O.; Austin, A. J.; Cammi, R.; Pomelli, C.; Ochterski, J. W.; Martin, R. L.; Morokuma, K.; Zakrzewski, V. G.; Voth, G. A.; Salvador, P.; Dannenberg, J. J.; Dapprich, S.; Daniels, A. D.; Farkas; Foresman, J. B.; Ortiz, J. V.; Cioslowski, J.; Fox, D. J., Gaussian 09, Revision B.01. Wallingford CT, 2009.

(21) Miertuš, S.; Scrocco, E.; Tomasi, J., Electrostatic interaction of a solute with a continuum. A direct utilizaion of AB initio molecular potentials for the prevision of solvent effects. *Chem. Phys.* **1981,** *55* (1), 117-129.

(22) Wang, J.; Wolf, R. M.; Caldwell, J. W.; Kollman, P. A.; Case, D. A., Development and testing of a general amber force field. *J. Comput. Chem.* **2004,** *25* (9), 1157-1174.

(23) Jakalian, A.; Bush, B. L.; Jack, D. B.; Bayly, C. I., Fast, efficient generation of high-quality atomic charges. AM1-BCC model: I. Method. *J. Comput. Chem.* **2000,** *21* (2), 132-146.

(24) Darden, T.; York, D.; Pedersen, L., Particle mesh Ewald: An N·log(N) method for Ewald sums in large systems. *J. Chem. Phys.* **1993,** *98* (12), 10089-10092.

(25) Miao, Y.; Sinko, W.; Pierce, L.; Bucher, D.; Walker, R. C.; McCammon, J. A., Improved Reweighting of Accelerated Molecular Dynamics Simulations for Free Energy Calculation. *J. Chem. Theory Comput.* **2014,** *10* (7), 2677-2689.

(26) PM6-optimized starting geometries are available from the ioChem-BD repository: https://doi.org/10.19061/iochem-bd-4-26